J. Fluid Mech. (1983), vol. 135, pp. 155–169
Printed in Great Britain

Vertical slender jets with surface tension

By JAMES F. GEER
State University of New York, Binghamton

AND JOHN C. STRIKWERDA
University of Wisconsin, Madison

(Received 6 January 1983 and in revised form 4 May 1983)

The shape of a vertical slender jet of fluid falling steadily under the force of gravity is studied. The problem is formulated as a nonlinear free boundary-value problem for the potential. Surface-tension effects are included and studied. The use of perturbation expansions results in a system of equations that can be solved by an efficient numerical procedure. Computations were made for jets issuing from three different orifice shapes, which were an ellipse, a square, and an equilateral triangle. Computational results are presented illustrating the effects of different values for the surface-tension coefficient on the shape of the jet and the periodic nature of the cross-sectional shapes.

1. Introduction

We wish to study the steady three-dimensional potential flow of a slender jet of fluid falling vertically in the presence of gravity. Our primary interest is to determine the shape of the free surface of the jet, given the cross-sectional shape and velocity profile of the jet at a particular height (e.g. at an orifice from which the jet emanates). We also wish to include surface-tension effects and evaluate their influence on the shape and spatial stability of the jet. Viscous effects are neglected.

This paper is an extension of our previous work on this problem (see Geer & Strikwerda 1980; Strikwerda & Geer 1981) to include the effects of surface tension. The mathematical formulation of the problem leads to a three-dimensional nonlinear boundary-value problem for Laplace's equation, for which the boundary of the flow is also unknown. However, for the case of a slender jet with surface-tension effects neglected, Tuck (1976) and Geer (1977*a*, *b*) derived equations to describe the first approximation to the cross-sectional shape and velocities of the jet. We shall show how this can be done with the effects of surface tension included. The problem of determining the shape is thus reduced to solving a nonlinear two-dimensional problem in the cross-sectional plane of the jet. Both Tuck and Geer gave an exact solution to this problem with surface-tension effects neglected, namely a jet with an elliptical cross-sectional shape. (See also Green (1977).) To date no other exact solutions have been found.

The purpose of this work is to present the results of solving numerically the associated nonlinear free boundary-value problem for jets issuing from orifices of several different shapes with surface-tension effects included. The problem is formulated in §2 and then transformed into a form more suitable for numerical integration. In §3, a numerical method, which we have used to integrate the problem outlined in §2, is briefly described. This method is an extension of a method we have described elsewhere (Strikwerda & Geer 1981), and it may be useful in solving other nonlinear free boundary-value problems.

In §4 we present the results of our calculations using two different values of the Weber number for the flow for each of three different orifice shapes. These shapes include an ellipse, a square, and an equilateral triangle. We discuss these results in §5, with special emphasis on the effects of surface tension on the cross-section shape and waves on the surface of the jet.

2. Formulation of the problem

Let the velocity potential of the jet be denoted by $\Phi = \Phi(r, \theta, z; \epsilon)$ and let the shape of the free surface of the jet be described by $r = \mathscr{S}(\theta, z; \epsilon)$ (see figure 1). Here r, θ and z form the usual (non-dimensional) cylindrical coordinate system, with the positive z-axis pointing vertically downward in the direction of gravity. The parameter ϵ, the slenderness ratio of the jet, is the ratio of a typical radius of the jet to a typical length along the jet, and is defined precisely by Geer (1977*a*). The boundary conditions at the free surface are the kinematic conditions of no flow through the surface and the jump in pressure due to surface tension. For small values of ϵ, we can show, using the ideas of Geer (1977*a*), that Φ and $\mathscr{S}$ are given by

$$\Phi = \tfrac{2}{3}(1+z)^{\frac{3}{2}} + \epsilon^2\phi(r, \theta, z) + O(\epsilon^4), \tag{2.1}$$

$$\mathscr{S} = S(\theta, z) + O(\epsilon^2), \tag{2.2}$$

where ϕ and S satisfy the conditions

$$\frac{\partial^2\phi}{\partial r^2} + \frac{1}{r}\frac{\partial\phi}{\partial r} + \frac{1}{r^2}\frac{\partial^2\phi}{\partial\theta^2} = -\tfrac{1}{2}(1+z)^{-\frac{1}{2}} \quad (z > 0, \quad 0 \leqslant r < S(\theta, z)), \tag{2.3}$$

with

$$\frac{\partial\phi}{\partial r} - \frac{1}{S^2}\frac{\partial S}{\partial\theta}\frac{\partial\phi}{\partial\theta} = (1+z)^{\frac{1}{2}}\frac{\partial S}{\partial z}, \tag{2.4}$$

$$\left(\frac{\partial\phi}{\partial r}\right)^2 + S^{-2}\left(\frac{\partial\phi}{\partial\theta}\right)^2 + 2(1+z)^{\frac{1}{2}}\frac{\partial\phi}{\partial z} = W^{-1}\frac{SS_{\theta\theta} - S^2 - 2S_\theta^2}{(S^2 + S_\theta^2)^{\frac{3}{2}}}, \tag{2.5}$$

holding on $r = S(\theta, z)$. Equation (2.3) follows from Laplace's equation for the potential, while (2.4) and (2.5) result from the substitution of the perturbation expansions (2.1) and (2.2) in the boundary conditions. In (2.5), W is defined by $W = 2g^2b^3\rho/\gamma U^2$, where g is the acceleration due to gravity, b^2 is the cross-sectional area of the jet at $z = 0$, ρ is the mass density of the fluid, γ is the surface-tension coefficient, and U is the velocity of the jet at $z = 0$. The Weber number for the jet is $\epsilon^{-4}W$. (See the appendix for a derivation of (2.5) and a discussion of the Weber number for this flow.) Thus we see that ϕ must satisfy the two-dimensional Poisson equation (2.3) in the cross-section of the jet, while (2.4) essentially prescribes the normal derivative of ϕ at the boundary of the cross-section. Equation (2.5) is the additional condition which is needed to determine the free surface.

To find ϕ and S, we transform the problem (2.3)–(2.5) into a form that is somewhat easier to deal with numerically. We first note that we can easily find a particular solution to (2.3) and consequently we write ϕ in the form

$$\phi = -\tfrac{1}{8}(1+z)^{-\frac{1}{2}}r^2 + \psi, \tag{2.6}$$

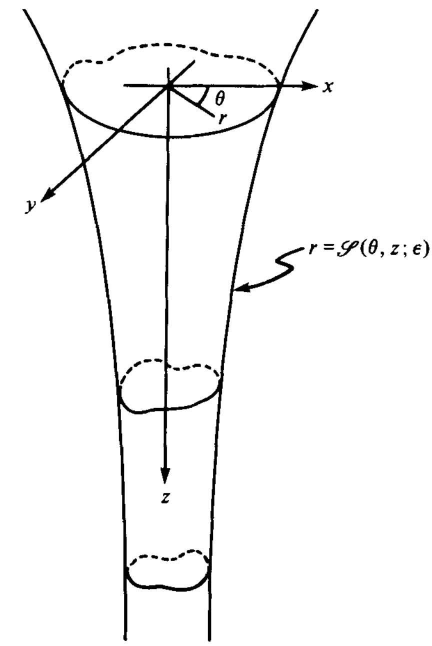

FIGURE 1. Sketch of a vertical slender jet, with an indication of the coordinate system. The locus of centroids of the cross-sections of the jet form a straight line (in the direction of gravity), which we choose to be the z-axis. Then r, θ and z form the usual cylindrical coordinate system, where θ is measured from any convenient plane through the z-axis. The free surface of the jet is denoted by $r = \mathscr{S}(\theta, z; \epsilon)$.

where ψ satisfies the homogeneous version of (2.3), i.e. Laplace's equation. Both ψ and S are presumed known at $z = 0$. We then introduce a new independent radial variable ρ, related to r by

$$\rho = \frac{r}{S(\theta, z)}. \tag{2.7}$$

Thus r is stretched in a non-uniform manner, but the unknown boundary $r = S(\theta, z)$ is mapped onto the known boundary $\rho = 1$. We also define the new dependent variable $R(\theta, z)$ by

$$R(\theta, z) = \tfrac{1}{2}S(\theta, z)^2 (1+z)^{\frac{1}{2}}. \tag{2.8}$$

In terms of the independent variables ρ, θ, and z, and the dependent variables $\psi(\rho, \theta, z)$ and $R(\theta, z)$, (2.4) and (2.5) can be written as

$$\frac{\partial R}{\partial z} = (1+\beta^2)\frac{\partial \psi}{\partial \rho} - \beta\frac{\partial \psi}{\partial \theta}, \tag{2.9}$$

$$4R\frac{\partial \psi}{\partial z} = (1+\beta^2)\left(\frac{\partial \psi}{\partial \rho}\right)^2 - \left(\frac{\partial \psi}{\partial \theta}\right)^2 - \frac{3}{4}\frac{R^2}{(1+z)^2} + W^{-1}(2R)^{\frac{1}{2}}(1+z)^{-\frac{1}{4}}\frac{\beta_\theta - 1 - \beta^2}{(1+\beta^2)^{\frac{3}{2}}}, \tag{2.10}$$

where

$$\beta = \frac{1}{S}\frac{\partial S}{\partial \theta} = \frac{1}{2}\frac{1}{R}\frac{\partial R}{\partial \theta}.$$

These equations hold for $\rho = 1$, $0 \leqslant \theta \leqslant 2\pi$ and $z > 0$. The differential equation (2.3) then becomes

$$(1+\beta^2)\frac{1}{\rho}\frac{\partial}{\partial \rho}\left(\rho\frac{\partial \psi}{\partial \rho}\right) - \frac{\partial \beta}{\partial \theta}\frac{1}{\rho}\frac{\partial \psi}{\partial \rho} + \frac{1}{\rho^2}\frac{\partial^2 \psi}{\partial \theta^2} - 2\beta\frac{1}{\rho}\frac{\partial^2 \psi}{\partial \rho\, \partial \theta} = 0$$

$$(0 \leqslant \theta \leqslant 2\pi, \quad 0 \leqslant \rho < 1, \quad z \geqslant 0). \tag{2.11}$$

As a consequence of (2.3)–(2.4), we find the integrability condition

$$\int_0^{2\pi} R(\theta, z)\,\mathrm{d}\theta = \text{constant}, \tag{2.12}$$

which expresses the constant mass flux in the jet.

Thus, we seek solutions to (2.9)–(2.11) for ψ and R in the region $0 \leqslant \rho \leqslant 1$, $z > 0$. Once ψ and R have been found, ϕ and S can be recovered using (2.6) and (2.8).

3. Method of solution

In this section we will briefly describe the method we have devised to solve the problem formulated in §2. This method is an extension of the method we have used to solve the problem when surface-tension effects are neglected, which we have discussed in detail elsewhere (see Strikwerda & Geer 1980).

In order to obtain a numerical approximation to the solution of our problem formulated in this manner, we use a finite-difference scheme defined on the grid points as follows:

$$\left.\begin{aligned} \theta_i &= (i-1)\,\Delta\theta \quad (i = 1, \ldots, N), \\ \rho_j &= 1-(j-1)\,\Delta\rho \quad (j = 1, \ldots, M), \\ z_n &= n\Delta z \quad (n = 0, 1, 2, 3, \ldots), \end{aligned}\right\} \tag{3.1}$$

where $\Delta\theta = 2\pi/(N-1)$, $\Delta\rho = 1/(M-1)$, and Δz is chosen to satisfy appropriate stability and accuracy criteria. Note that $\theta_1 = 0$, $\theta_N = 2\pi$, $z_0 = 0$, $\rho_1 = 1$ and $\rho_M = 0$. We then use the MacCormack (1969) scheme with a special time-splitting to solve (2.9) and (2.10). In particular, if we define the vector $\boldsymbol{w}(\theta, z)$ by $\boldsymbol{w} = (R, \psi)^{\mathrm{T}}$, then (2.9) and (2.10) can be written as

$$\frac{\partial \boldsymbol{w}}{\partial z} = \boldsymbol{F}\left(z, \boldsymbol{w}, \frac{\partial \boldsymbol{w}}{\partial \theta}, \frac{\partial \psi}{\partial \rho}\right) + \boldsymbol{G}\left(z, R, \frac{\partial R}{\partial \theta}, \frac{\partial^2 R}{\partial \theta^2}\right), \tag{3.2}$$

where $\boldsymbol{F}$ contains all the terms from the right-hand sides of (2.9) and (2.10), except those from (2.10) that are multiplied by W^{-1}, and $\boldsymbol{G}$ contains the terms from (2.10) multiplied by W^{-1}. Using the usual forward- and backward-difference operators D_+ and D_- respectively, and the centred second-difference operator D^2, the forward–backward MacCormack scheme is given by the following formulas:

(predictor)

$$\left.\begin{aligned} \tilde{\boldsymbol{W}}_i^{n+\frac{1}{2}} &= \boldsymbol{W}_i^n + \Delta z \boldsymbol{F}(z_n, \boldsymbol{W}_i^n, \mathrm{D}_+ \boldsymbol{W}_i^n, \mathrm{D}_\rho \psi_i^n), \\ \tilde{\boldsymbol{W}}_i^{n+1} &= \tilde{\boldsymbol{W}}_i^{n+\frac{1}{2}} + \Delta z \boldsymbol{G}(z_n, \tilde{R}_i^{n+\frac{1}{2}}, \mathrm{D}\tilde{R}_i^{n+\frac{1}{2}}, \mathrm{D}^2\tilde{R}_i^{n+\frac{1}{2}}); \end{aligned}\right\} \tag{3.3}$$

(corrector)

$$\left.\begin{aligned} \boldsymbol{W}_i^{n+\frac{1}{2}} &= \tfrac{1}{2}\{\boldsymbol{W}_i^n + \tilde{\boldsymbol{W}}_i^{n+1} + \Delta z \boldsymbol{F}(z_{n+1}, \tilde{\boldsymbol{W}}_i^{n+1}, \mathrm{D}_- \tilde{\boldsymbol{W}}_i^{n+1}, \mathrm{D}_\rho \tilde{\psi}_u^{n+1})\}, \\ \boldsymbol{W}_i^{n+1} &= \boldsymbol{W}_i^{n+\frac{1}{2}} + \tfrac{1}{2}\Delta z \boldsymbol{G}(z_{n+1}, R_i^{n+\frac{1}{2}}, \mathrm{D}R_i^{n+\frac{1}{2}}, \mathrm{D}^2 R_i^{n+\frac{1}{2}}). \end{aligned}\right\} \tag{3.4}$$

In order to maintain symmetry, the forward–backward MacCormack scheme is alternated with the backward–forward scheme, which uses backward differences in the predictor step and forward differences in the corrector step. Also, it was found that the conservation law (2.12) was satisfied more closely when the quantity β in (2.9) and (2.10) was approximated as

$$D_\pm R_i^n/(R_i + R_{i\pm 1}),$$

and this form was used in all the calculations given here.

The expression $\mathrm{D}R$ used in (3.3) and (3.4) in the $\boldsymbol{G}$-operator is used to denote the difference approximation to $\partial R/\partial\theta$ which appears in $\boldsymbol{G}$ only in the quantity β. The approximation for β is given by

$$\beta_i^2 = \left(\frac{1}{2}\frac{1}{R}\frac{\partial R}{\partial \theta}\right)_i^2 \approx \frac{1}{2}\left\{\left(\frac{\mathrm{D}_+ R_i}{R_i+R_{i+1}}\right)^2+\left(\frac{\mathrm{D}_- R_i}{R_i+R_{i-1}}\right)^2\right\}. \tag{3.5}$$

The term $\mathrm{D}_\rho \psi_i^n$ in (3.3) and (3.4) is an approximation to $\partial\psi/\partial\rho$ on $\rho = 1$ at $\theta = \theta_i$ and $z = z_n$. It is computed by first solving for an approximation to the solution ψ of (2.11), with ψ_i^n specified on the boundary. The approximation is given by equations (3.6) and (3.7) of Geer & Strikwerda (1980), which are solved by successive over-relaxation. The term $\mathrm{D}_\rho \psi_i^n$ is then approximated by a second-order one-sided approximation to $\partial\psi/\partial\rho$ given by equation (3.8) of Geer & Strikwerda (1980).

Equations (3.1)–(3.5) above and equations (3.6)–(3.8) of Geer & Strikwerda (1980) describe our numerical scheme to solve the problem of §2. The scheme can be shown to be second-order accurate in both θ and z (see Strikwerda & Geer 1980).

The splitting of the right-hand sides of (2.9) and (2.10) into the $\boldsymbol{F}$- and $\boldsymbol{G}$-operators and the method used in (3.3) and (3.4) allows the use of much larger values of Δz in the calculations. Note that the second operation in each step determines the boundary values of the potential using the most recent values of R. Thus it is similar to an implicit method, but is, in fact, explicit. In the calculations using the above splitting, the choice of Δz was limited only by the accuracy required to resolve the oscillations of the jet. Without this splitting, the choice of Δz was limited by a stability condition, which was much more severe than the accuracy limitation using the splitting.

4. Examples

Several examples of thin streams falling vertically through an orifice of a specified shape were calculated using the scheme outlined in §3. For each example the initial conditions were $\psi \equiv 0$ and $R(\theta, z)$, i.e. $S(\theta, z)$ specified at $z = 0$. Note that the condition $\psi = 0$ at $z = 0$ corresponds to a jet that is emanating with a cross-sectional velocity profile determined by the potential $-\frac{1}{8}(1+z)^{-\frac{3}{2}} r^2$. Thus, in the notation of §3, we set $\psi_{i,j}^0 = 0$ and $R_i^0 = R^0(\theta_i)$ at $z = 0$, where $R^0(\theta)$ was specified by one of the following (see figures 2–4):

(1) an ellipse $R^0 = \pi^{-1}(0.25\cos^2\theta + \sin^2\theta)^{-1}$, where the semi-axes of the ellipse are $2(2/\pi)^{\frac{1}{2}}$ and $(2(\pi)^{\frac{1}{2}}$;

(2) an equilateral triangle $R^0 = (2/3^{\frac{3}{2}})\min_{l=0,1,2}\sec^2(\theta - \frac{2}{3}\pi l)$ where the length of the side of the triangle is $\frac{4^{\frac{1}{2}}}{3^{\frac{1}{4}}}$;

(3) a square $R^0 = \frac{1}{2}\min(\sec^2\theta, \operatorname{cosec}^2\theta)$, where the length of the side of the square is 2.

Each example has initial cross-sectional area of 4 and hence by (2.12) the areas are also equal for each value of $z > 0$.

For each example, the origin was located at the centre of mass of the shape, as required in the derivation of the basic equations (2.3)–(2.5) (see Geer 1977*a*). Each example was run for two values of W, namely 1 and 0.5. Figures 2–4 show cross-sections of the jet at several values of z between 0 and 2. For comparison, these figures may be compared with the corresponding figures when surface-tension effects are neglected, i.e. when W is infinite, in Geer & Strikwerda (1980).

Each of our examples was integrated much further in the z-direction than indicated in figures 2–4. In each case the cross-sectional shapes exhibited a periodic

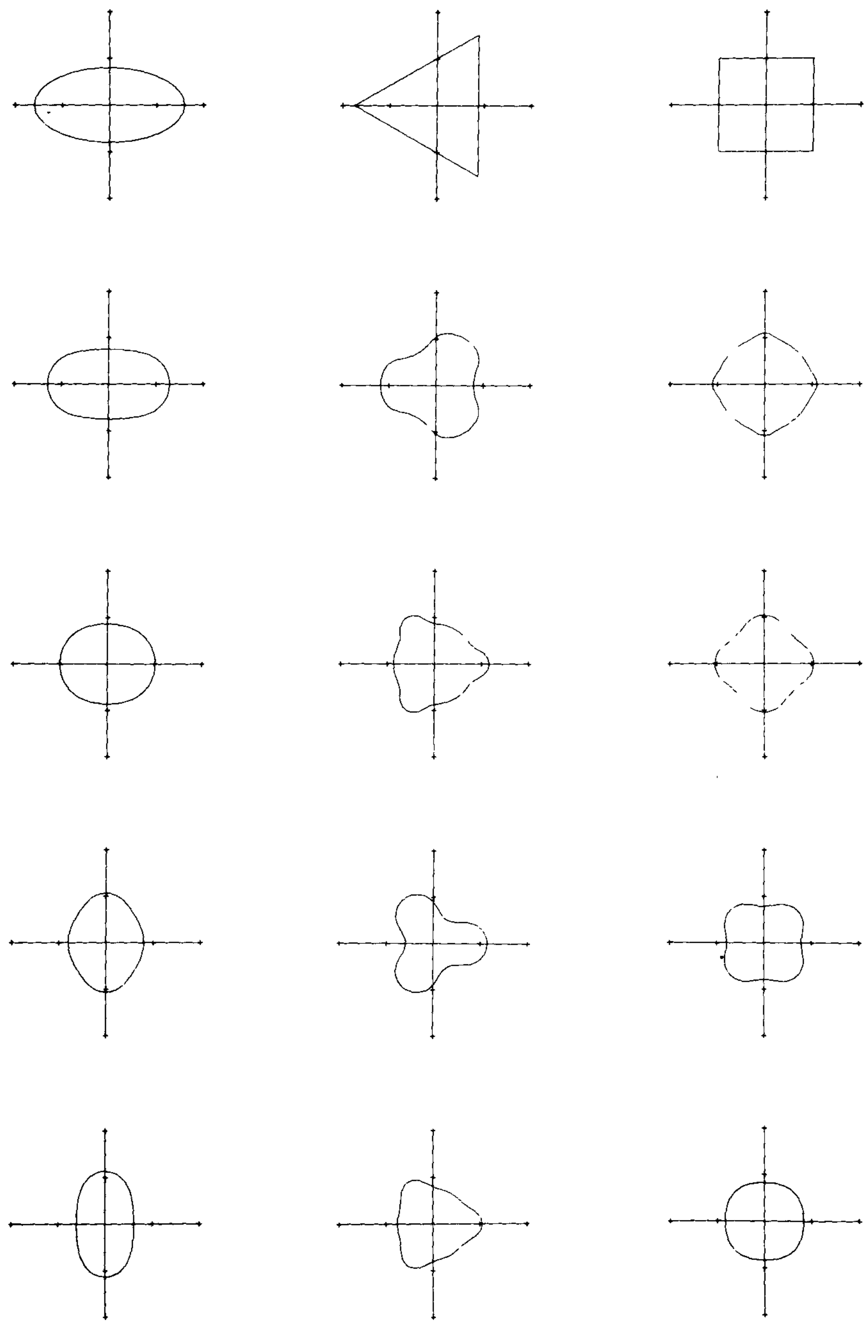

FIGURE 2. Cross-sectional shapes at several values of z of a jet with an initial shape in the form of an ellipse, a triangle or a square. The shapes are shown at $z = 0$, (0.5), 2 with $W = 1.0$.

behaviour in z, except for the gradual decrease in area due to gravitational acceleration. To exhibit this behaviour, we have plotted in figures 5 and 6 the values of $S(\theta, z)$, for two fixed values of θ, as a function of z. In these figures the definite wave structure of the jet can be seen. Representative cross-sectional shapes for each of our examples for larger values of z are shown in figures 7 and 8.

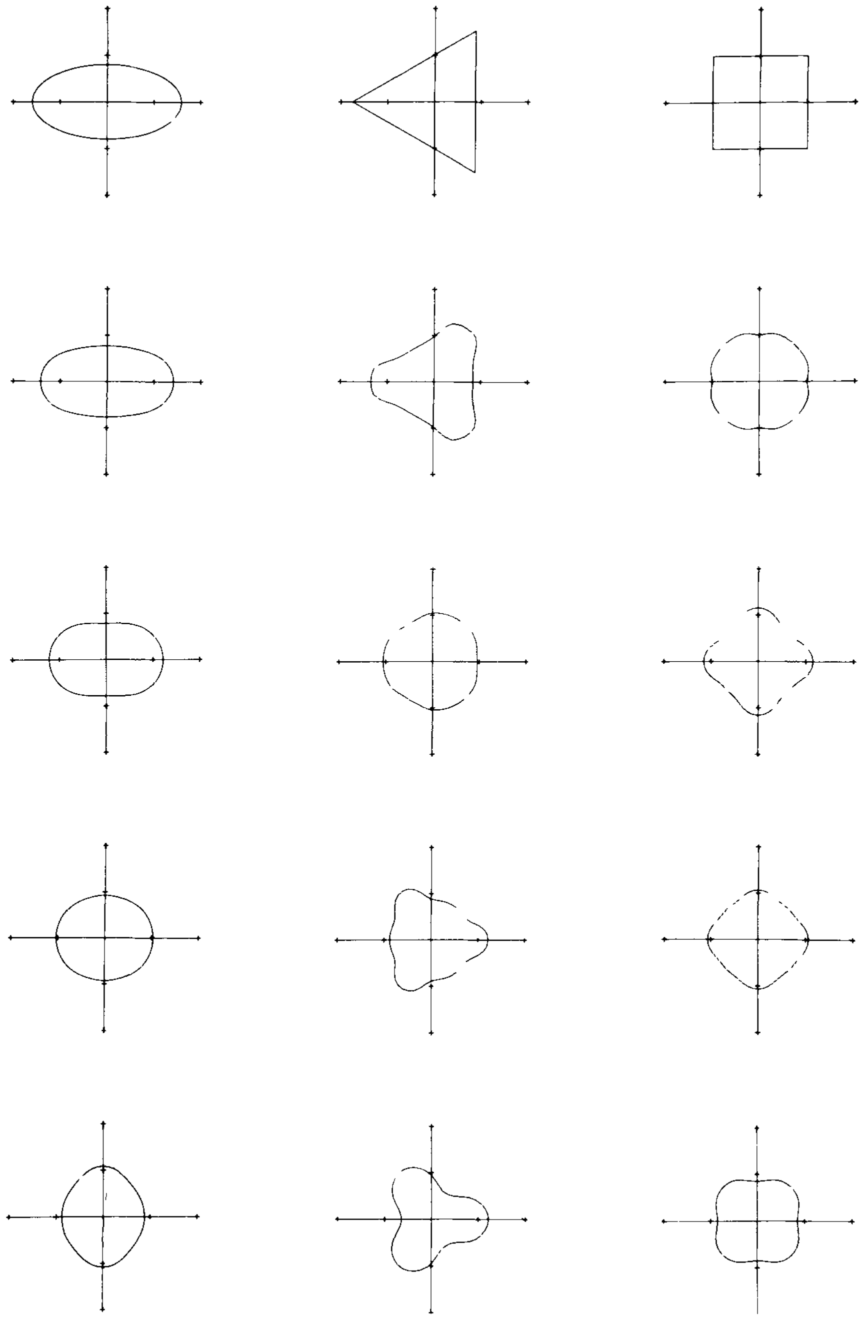

FIGURE 3. Cross-sectional shapes at several values of z of a jet with an initial shape in the form of an ellipse, a triangle or a square. The shapes are shown at $z = 0$, (0.25), 1 and with $W = 0.5$, which corresponds to a larger surface-tension coefficient.

5. Analysis of the waves

We now consider in more detail the wave behaviour of the slender jets we have calculated. Rayleigh (1879) has discussed waves on slender jets with surface tension (and gravity neglected) and has argued that the temporal frequency of the waves

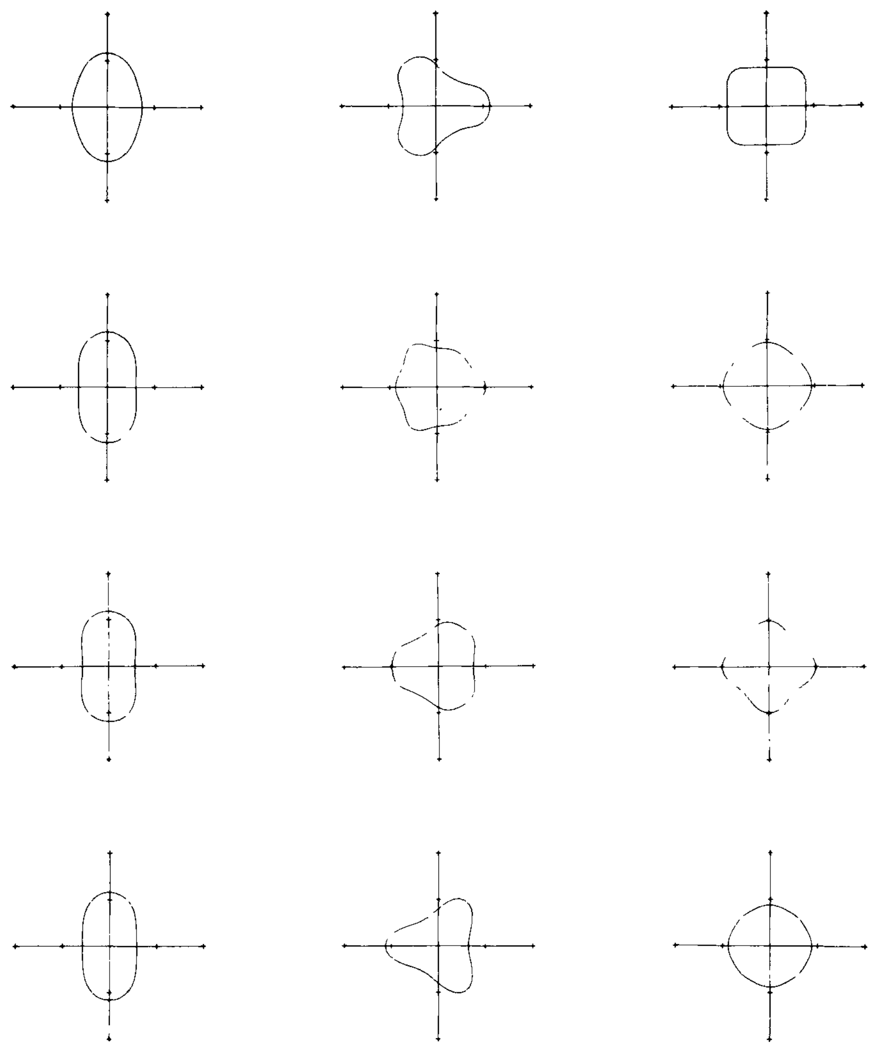

FIGURE 4. Continuation of figure 3 for z = 1.25, (0.25), 2.0.

should be proportional to the inverse square root of the Weber number W. He has also argued that if the dominant term in the Fourier expansion of the cross-sectional shape is

$$S \sim S_0 + S_1 \cos n(\theta - \theta_0)$$

then the temporal frequency must be proportional to

$$W^{-\frac{1}{2}}(n^3 - n)^{\frac{1}{2}}. \tag{5.1}$$

A similar argument shows that the spatial wavelength λ of the waves will be inversely proportional to the quantity in (5.1).

In order to investigate this relationship for the jet shapes computed here, we fit the curves of figures 5 and 6 to curves of the form

$$(1+z)^{-\frac{1}{4}}(a_0 + a_1 \sin(a_2 z + a_3)), \tag{5.2}$$

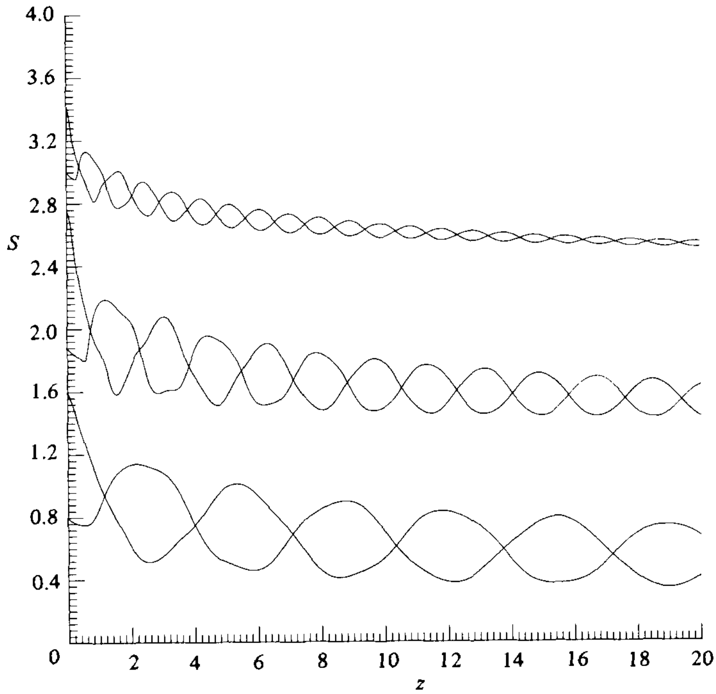

FIGURE 5. Plots of the values of $S(\theta, z)$ for $0 \leqslant z \leqslant 20$ for each of the three jet shapes and for two specific values of θ. For the ellipse, S was plotted for $\theta = 0$ and $\frac{1}{2}\pi$; for the triangle, $\theta = 0$ and $\frac{1}{3}\pi$; and for the square, $\theta = 0$ and $\frac{1}{4}\pi$. The value of W is 1.0. The lower pair of curves are for the ellipse, the middle pair are for the triangle, and the upper pair are for the square. For display purposes, the middle curves have been offset by 1.0 and the upper curves by 2.0.

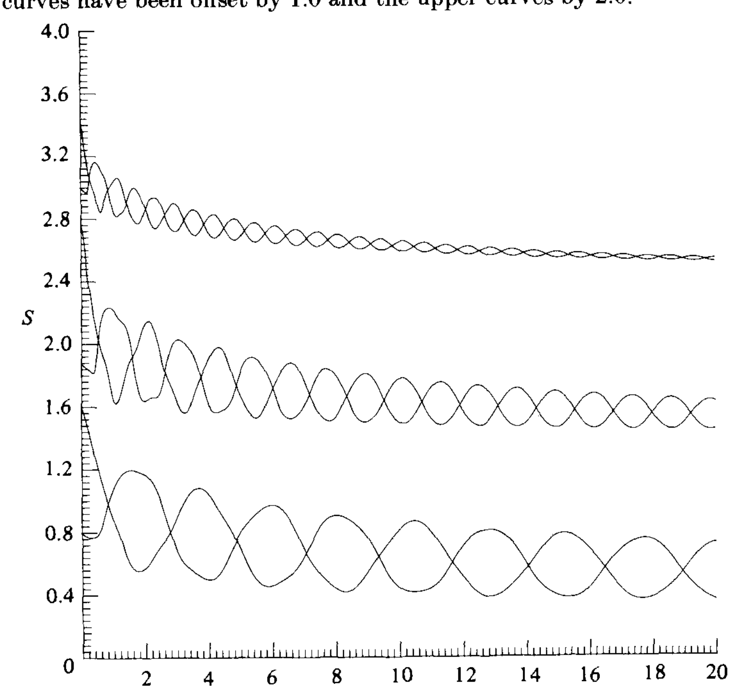

FIGURE 6. Same type of plot as in figure 5, except that W is now 0.5, corresponding to an increased surface-tension coefficient.

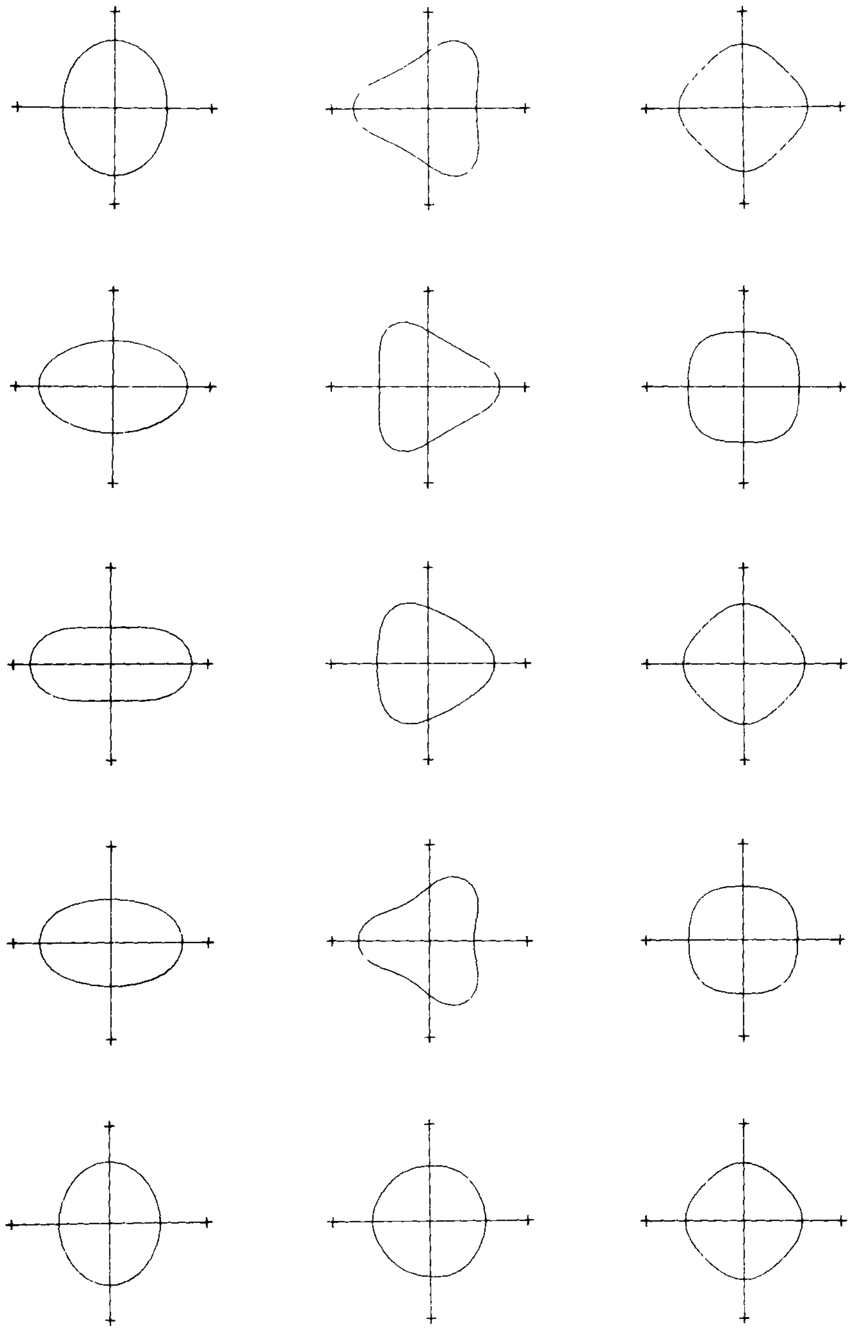

FIGURE 7. Cross-sectional shapes of the three jets at larger values of z. The shapes are shown for $z = 10$, (1), 14 and with $W = 1.0$.

where each a_j is a constant. The fitting was done by the least-squares method, using the routine NL2SOL written by Gay and described by Dennis, Gay & Welsch (1981). The approximate wavelength of the waves in figures 5 and 6 is then given by

$$\lambda = 2\pi/a_2.$$

The least-squares fit was done using all of the data displayed in figures 5 and 6, and also with only the data between $z = 10$ and $z = 20$. The use of only the second

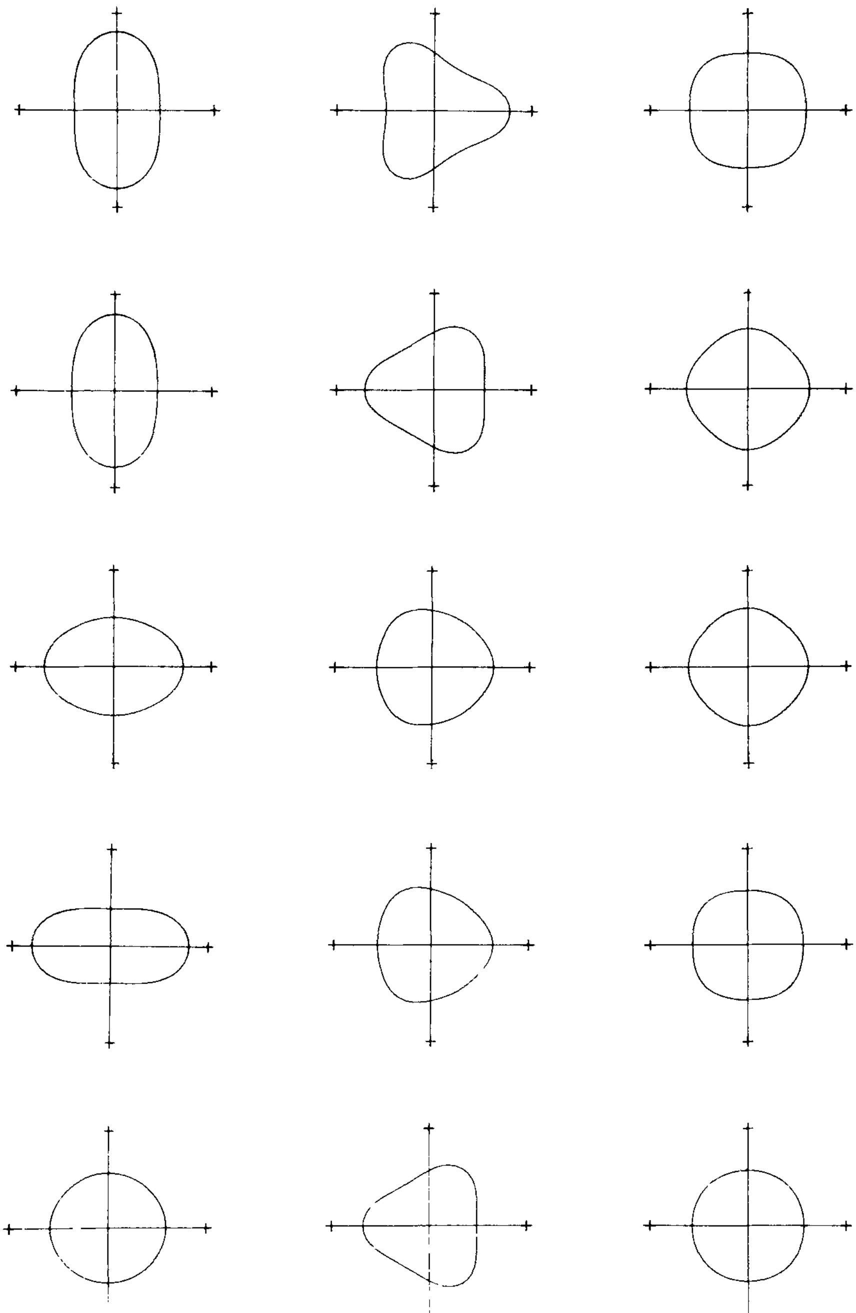

FIGURE 8. Same type of cross-sectional shapes as in figure 7, but with $W = 0.5$, representing an increase in the surface-tension coefficient.

half of the data was done to help eliminate the effects of any initial (spatial) transient disturbances, as well as to help determine whether or not the wavelength increased or decreased as a function of z. The results of the least-squares fit are displayed in table 1.

Two conclusions can be drawn from table 1. First, for each shape, the wavelength is essentially the same for each of the two curves (corresponding to different values

Shape	$W = 1.0$		$W = 0.5$	
	All data	Half data	All data	Half data
Ellipse				
0°	6.48	6.90	4.55	4.84
90°	6.48	6.91	4.55	4.86
Triangle				
0°	3.40	3.54	2.34	2.43
60°	3.39	3.54	2.34	2.43
Square				
0°	1.89	1.99	1.33	1.41
45°	1.89	1.99	1.32	1.41

TABLE 1. Estimates of the wavelengths for the curves in figures 5 and 6. The estimates are based on a least-squares fit using all of the data for $0 \leqslant z \leqslant 20$ and also using only the data for $10 \leqslant z \leqslant 20$. For each shape, the wavelengths were computed for each of the two curves corresponding to the two values of θ considered.

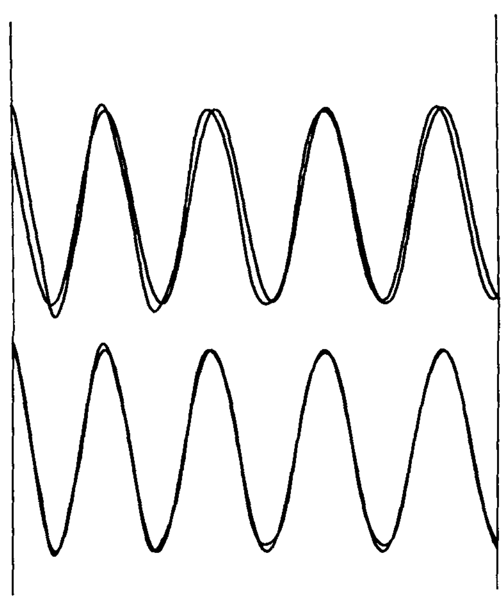

FIGURE 9. Comparison of the curve in figure 6 (multiplied by $(1+z)^{\frac{1}{4}}$) corresponding to the initially elliptical shape for $\theta = 0$ and $W = 0.5$ with the fitted curves: (*a*) form (5.2); and (*b*) form (5.4). The upper pair is the data compared with the form (5.2), and the lower pair is the data compared with the form (5.4).

of θ) shown in figures 5 and 6. Secondly, the wavelength is apparently increasing with z. This second conclusion is based upon the observation that the values obtained from using the latter half of the data are consistently larger than the values obtained by using all the data. (This also follows from an inspection of the curves of figures 5 and 6 when superimposed on the results of the least-squares fit, as in figure 9, which will be discussed below.)

To investigate Rayleigh's conclusions further, we also computed the quantity

$$\lambda_0 = \lambda W^{-\frac{1}{2}}(n^3 - n)^{\frac{1}{2}} \tag{5.3}$$

for each of the shapes we considered, with n equal to 2, 3 or 4 for the ellipse, triangle and square respectively. The values of λ_0 are displayed in table 2, both for the fit

Shape	$W = 1.0$ All data	$W = 1.0$ Half data	$W = 0.5$ All data	$W = 0.5$ Half data
Ellipse	2.53	2.70	2.51	2.67
Triangle	2.65	2.76	2.58	2.68
Square	2.33	2.45	2.31	2.46

TABLE 2. Values of λ_0 calculated from (5.3) for the curves of figures 5 and 6

using all of the data and also for the fit using only half of the data. (Since the two values of λ, corresponding to the different values of θ, are quite close for each of the shapes, the average was used to compute λ_0 in table 2.)

The results given in table 2 are certainly consistent with the idea that the wavelength is proportional to $W^{-\frac{1}{2}}$. In addition, the dependence of the wavelength on n is in quite good agreement with Rayleigh's analysis, considering the crudeness of our assignment of n as 3 for the triangle and 4 for the square.

Using the results above as a guide, we now show that the shape of the curves in figures 5 and 6 can be better approximated by curves of the form

$$(1+z)^{-\frac{1}{4}}\{b_0+b_1 \sin (b_2\, W^{-\frac{1}{2}}(1+z)^{\frac{7}{8}}+b_3)\} \tag{5.4}$$

than by curves of the form (5.2). We note that the form (5.4) corresponds to a shape with a slowly increasing wavelength proportional to $(1+z)^{\frac{1}{8}}$.

A plausibility argument for the form (5.4) is as follows. If we replace $S(\theta,z)$ in (2.4) and (2.5) by $(1+z)^{-\frac{1}{4}}\tilde{S}(\theta,z)$, these equations become

$$(1+z)^{-\frac{1}{4}}\frac{\partial\phi}{\partial r}-\frac{1}{\tilde{S}^2}\frac{\partial\tilde{S}}{\partial\theta}\frac{\partial\phi}{\partial\theta}=\frac{\partial\tilde{S}}{\partial z}-\tfrac{1}{4}\tilde{S}(1+z)^{-1}, \tag{5.5}$$

$$\left((1+z)^{-\frac{1}{4}}\frac{\partial\phi}{\partial r}\right)^2+\frac{1}{\tilde{S}^2}\left(\frac{\partial\phi}{\partial\theta}\right)^2+2\frac{\partial\phi}{\partial z}=W^{-1}(1+z)^{-\frac{1}{4}}\frac{\tilde{S}\tilde{S}_{\theta\theta}-\tilde{S}^2-2\tilde{S}_\theta^2}{(\tilde{S}^2+\tilde{S}_\theta^2)^{\frac{3}{2}}}. \tag{5.6}$$

If we now assume that, for large z, $\tilde{S}$ behaves like $f_1(\mu(1+z)^\beta+\delta(\theta),\theta)$, where $\beta>0$, then from (5.5) we see that at least one of the terms $(1+z)^{-\frac{1}{4}}\partial\phi/\partial r$ or $\partial\phi/\partial\theta$ must behave like $\mu(1+z)^{\beta-1}f_2(\mu(1+z)^\beta+\delta(\theta),\theta)$, as z becomes large. Using this result in (5.6), we find that $\mu^2(1+z)^{2(\beta-1)}$ must be proportional to $W^{-1}(1+z)^{-\frac{1}{4}}$. Thus μ is proportional to $W^{-\frac{1}{2}}$ and $2(\beta-1)=-\frac{1}{4}$, or $\beta=\frac{7}{8}$.

Table 3 displays the values of b_2 obtained for each of our jets using all or half of the data. The better agreement among the values of b_2 in each row than among the values of λ in table 1 supports the conjecture that the form (5.4) is more appropriate than the form (5.2) and hence that the wavelength is proportional to $W^{\frac{1}{2}}(1+z)^{\frac{1}{8}}$. Also, the least-squares fits using (5.4) were noticeably better than those using (5.2) when superimposed on the original curves (see figure 9).

Stimulated by our conjecture (5.4), Keller (1983) has shown that small perturbations of a circular jet do indeed have wavelengths asymptotically proportional to $W^{-\frac{1}{2}}(1+z)^{\frac{1}{8}}$.

In addition to the effects we have discussed here, there was also a small decrease in the amplitudes of the curves beyond the factor of $(1+z)^{-\frac{1}{4}}$. This decrease was smallest for the ellipse and greatest for the square. It is difficult to determine whether this decrease in amplitude is due to numerical dissipation or is actually part of the exact solution.

Shape	$W = 1.0$ All data	$W = 1.0$ Half data	$W = 0.5$ All data	$W = 0.5$ Half data
Ellipse				
0°	1.465	1.464	1.478	1.483
90°	1.469	1.462	1.478	1.478
Triangle				
0°	2.804	2.862	2.863	2.948
60°	2.801	2.860	2.862	2.949
Square				
0°	4.977	5.081	4.989	5.065
45°	4.975	5.079	4.988	5.066

TABLE 3. Values of the parameter b_2 in (5.4) for different jets

The first author was partially supported by the Research Foundation of SUNY under Contract no. 240-6135A and partially supported under NASA Contract no. NAS1-14101. The research for the second author was supported in part under NASA Contract no. NAS1-14101 while he was in residence at the Institute for Computer Applications in Science and Engineering, NASA Langley Research Center, Hampton, VA 23665, and in part by the United States Army under Contract no. DAAG29-80-C-0041.

Appendix

In this appendix we show briefly how (2.5) is derived. At a free surface, the jump in pressure $\Delta P = P - P_a$ due to surface tension is given by

$$P - P_a = \gamma\left(\frac{1}{R_1} + \frac{1}{R_2}\right), \tag{A 1}$$

where $R_1^{-1} + R_2^{-1}$ is twice the mean curvature of the surface, P is the pressure within the jet and P_a is the (constant) pressure of the surrounding atmosphere. In particular, if the equation of our surface is of the form $\bar{r} = h(\theta, \bar{z})$, where $\bar{r}, \theta$ and $\bar{z}$ form the usual cylindrical coordinate system, then we find

$$\frac{1}{R_1} + \frac{1}{R_2} = -[h^2(1+h_z^2)+h_\theta^2]^{-\frac{3}{2}}\{hh_{zz}(h^2+h_\theta^2) - 2(hh_{\theta z} - h_z h_\theta)\, h_z h_\theta + (1+h_z^2)\,(hh_{\theta\theta} - 2h_\theta^2 - h^2)\}. \tag{A 2}$$

Using the notation of Geer (1977 *a*) and introducing non-dimensional variables $r = \bar{r}/b$ and $z = \bar{z}/L$, where $L = U^2/2g$, and letting $h = bS(\theta, z)$, we find that (A 2) can be written as

$$\frac{1}{R_1} + \frac{1}{R_2} = \frac{1}{b}\frac{S^2 + 2S_\theta^2 - SS_{\theta\theta}}{(S^2+S_\theta^2)^{\frac{3}{2}}} + O(\epsilon^2 b^{-1}), \tag{A 3}$$

where $\epsilon = b/L$. Also, if $\Phi = UL\phi$ is the velocity potential for the flow within the jet, we can use Bernoulli's theorem and (A 3) to write (A 1) as

$$\left(\frac{\partial\phi}{\partial r}\right)^2 + \frac{1}{S^2}\left(\frac{\partial\phi}{\partial\theta}\right)^2 + \epsilon^2\left(\frac{\partial\phi}{\partial z}\right)^2 = \epsilon^2(1+z) + \tilde{W}^{-1}\frac{SS_{\theta\theta} - S^2 - 2S_\theta^2}{(S^2+S_\theta^2)^{\frac{3}{2}}} + O(\epsilon^2\tilde{W}^{-1}), \tag{A 4}$$

where $\tilde{W}$ is the Weber number for our flow, defined by

$$\tilde{W} = \frac{\rho U^2 b}{2\gamma\epsilon^2} = \frac{\rho U^6}{8\gamma b g^2}. \tag{A 5}$$

(Equation (A 4) is a generalization of equation (11) in Geer (1977*a*), which includes surface-tension effects for a slender vertical jet.)

Now, following the same procedure as Geer (1977*a*), we let $\phi = \phi^0 + \epsilon\phi^1 + \epsilon^2\phi^2 + \dots$ and see from his equations (7) and (9) that ϕ^0 and ϕ^1 are functions of z alone, and, in particular, do not depend upon r or θ. Thus the lowest-order terms on the left-hand side of (A 4) which can vary with θ are $O(\epsilon^4)$. Hence a meaningful condition on S can be obtained from (A 4) only if $\tilde{W}^{-1} = O(\epsilon^4)$, i.e.

$$\tilde{W}^{-1} = \epsilon^4 W^{-1}, \quad W^{-1} = O(1), \tag{A 6}$$

where $W = \epsilon^4 \tilde{W} = 2g^2b^3\rho/\gamma U^2$. Using (A 6) and the expansions (2.1) and (2.2), the terms that are $O(\epsilon^4)$ in (A 4) yield (2.5).

REFERENCES

Dennis, J. E., Gay, D. M. & Welsch, R. E. 1981 An adaptive nonlinear least-squares algorithm. *ACM Trans. Math. Software* **7**, 348–368.

Geer, J. F. 1977*a* Slender streams with gravity: outer asymptotic expansions I. *Phys. Fluids* **20**, 1613–1621.

Geer, J. F. 1977*b* Slender streams with gravity: outer asymptotic expansions II. *Phys. Fluids* **20**, 1622–1630.

Geer, J. F. & Strikwerda, J. C. 1980 Vertical slender jets. *J. Fluid Mech.* **101**, 53–63.

Green, A. E. 1977 On the steady motion of jets with elliptical sections. *Acta Mech.* **26**, 171–177.

Keller, J. B. 1983 Capillary waves on a vertical jet. *J. Fluid Mech.* **135**, 171–173.

MacCormack, R. W. 1969 The effect of viscosity in hypervelocity impact cratering. *AIAA Hypervelocity Impact Conf.*, April 1969; *AIAA Paper* 69–354.

Rayleigh, Lord 1879 On the capillary phenomena of jets. *Proc. R. Soc. Lond.* **29**, 71–97.

Rayleigh, Lord 1945 *The Theory of Sound*, 2nd edn. Dover.

Strikwerda, J. C. & Geer, J. F. 1980 A numerical method for computing the shape of a vertical slender jet. *SIAM J. Sci. Statist. Comput.* **1**, 449–466.

Tuck, E. O. 1976 The shape of free jets of water under gravity. *J. Fluid Mech.* **76**, 625–640.